Since January 2020 Elsevier has created a COVID-19 resource centre with free information in English and Mandarin on the novel coronavirus COVID-19. The COVID-19 resource centre is hosted on Elsevier Connect, the company's public news and information website.

Sustainable Cities and Society 62 (2020) 102405

Contents lists available at ScienceDirect

Sustainable Cities and Society

journal homepage: www.elsevier.com/locate/scs

Sustainable design of courtyard environment: From the perspectives of airborne diseases control and human health

Jiawei Leng[a,*], Qi Wang[b], Ke Liu[a]

[a] School of Architecture, Southeast University, Sipailou, Nanjing, 210096 China
[b] Architects & Engineers Co. Ltd. of Southeast University, Sipailou, Nanjing, 210096, China

ARTICLE INFO

Keywords:
Courtyard environment
Design
Infection risk
Airborne disease control
Simulations

ABSTRACT

Courtyards have functioned as an effective passive architectural design strategy for various climate conditions, especially popular in hot-humid climates. Sustainable and delicate designs are necessary to create safe, healthy and comfortable courtyard environment. Most of the available literature focused on thermal comfort for courtyard, and the researches towards air pollution/disease control was rare. Further considering the severe impact of COVID-19 crisis, the current study aims to develop a numerical strategy to optimize physical environment in courtyard, including distributions of airborne pollutant, drought sensation and infection risk. Experimental data from literature was used to validate the numerical models. The evaluation indexes were adopted for the assessment of draft sensation, pollution exposure risk etc. The influences of geometric design parameters (i.e., courtyard width, height etc.) were investigated, and courtyard width (D) was the most sensitive parameter. If D increased from 5.8 m to 11.8 m, average air pollutant concentration decreased by 80 %, while drought sensation increased by 30 %. In static wind conditions, infection possibility (with R value up to 3 %) in courtyard was comparable to those in indoor environments during the COVID-19 period. This work will be of great importance for sustainable development of courtyards from the perspectives of airborne diseases control.

1. Introduction

Courtyard space plays an important role in the traditional residential texture in China for dealing with the local climate and human comfort need (Hao, Yu, Xu, & Song, 2019), and it is still an essential activity platform for life habits in some countries (Khalili & Amindeldar, 2014; Soflaei, Shokouhian, Abraveshdar, & Alipour, 2017). Even though a courtyard space is part of the residential texture, it may be shared by multiple families, such as traditional quadrangle courtyard in China. Besides, traditional courtyard spaces are also valuable tourism resources (Giorgi, Cattaneo, Ni, & Alatriste, 2020). Therefore, the courtyard can be treated as a public space, and public safety (e.g. infectious disease, fire safety) is an important factor in architecture design.

With the fast social and economic development, traditional villages and towns are under the influence of the change of modern lifestyle and rapid urbanization, facing the various practical problems, i.e., the contradiction between the living environment with high densities of buildings and the requirements of higher living standard. Optimal courtyard design is an efficient and sustainable strategy to improve thermal and micro-climatic conditions (Zahra, Shahin, & Pirouz, 2018). Sustainable courtyard environment should contain the characteristics of safety, health, comfort and energy-saving, which are closely correlated with the distribution and dispersion of surrounding parameters (Teshnehdel, Mirnezami, Saber, Pourzangbar, & Olabi, 2020; Yang, Liu, Qian, & Niu, 2020), i.e., airflow, temperature, pollutant concentration, humidity etc. The rapid spread of the infection and the high level of morbidity associated with the COVID 19 epidemic is calling for appropriate control measures (Xu, Luo, Yu, & Cao, 2020), which also inspires and encourages the well design of all functioning living environments for future prevention of disease-infectious alike crisis. To the best knowledge, this is rarely concerned in many buildings especially for courtyards design, i.e., air pollution and airborne disease control.

Recently, many researchers investigated physical environments in courtyard, mainly focusing on thermal environment and occupant comfort. Previous study conducted field experiments in 16 traditional Chinese shop-houses (Kubota, Zakaria, Abe, & Toe, 2017), it was found that air temperatures in internal courtyards were significantly influenced by the sky view factor, courtyard height and building height. These design parameters are very essential in architectural design. Similarly, long-term field monitoring (about two-years) proved that the

* Corresponding author.
E-mail address: jw_leng@seu.edu.cn (J. Leng).

https://doi.org/10.1016/j.scs.2020.102405
Received 14 June 2020; Received in revised form 11 July 2020; Accepted 14 July 2020
Available online 17 July 2020

lifespan of courtyard building also influenced the thermal comfort (Carlos, Eduardo, Carmen, & Victoria., 2019).

Ventilation performances in courtyard environment were also investigated by numerical and experimental methods (Hao et al., 2019). Based on opening characteristics, courtyard could be regarded as enclosed cavities, and a set of large-eddy simulations were utilized to simulate the effects of lateral openings on ventilation in courtyards with different configurations (Gronemeier & Sühring, 2019). Previous research optimized design of opening level of courtyards by CFD (Computational Fluid Dynamics) simulation and experimental measurement to improve natural ventilation performance in hot summer and cold winter (HSCW) climate zones (Hao et al., 2019). To improve natural ventilation and thermal comfort in courtyards, courtyard layout, aspect ratio, height-width ratio and southward orientation were optimized by numerical simulations (Nasrollahi, Hatami, Khastar, & Taleghani, 2017; Xu, Luo, Wang, Hong, & Fu, 2018). Similarly, the influences of opening angles/distributions, incoming wind orientations and courtyard height on ventilation performance and comfort level were also simulated by using CFD method (Micallef, Buhagiar, & Borg, 2016; Mousa, Lang, & Auer, 2017; Subhashini & Thirumaran, 2019). Except for architectural optimization design, numerical simulations were also adopted to design shading, planting and HVAC devices to improve thermal environment in courtyard (Li et al., 2019; Taleb, Wriekat, & Hashaykeh, 2020). The available literature described above mainly focused on thermal environment and ventilation performance in courtyard. The researches on airborne pollutant/disease control were insufficient. Reducing air pollutant exposure is very essential in built environment (Hvelplund et al., 2019), especially in COVID-19 epidemic. Sustainable and delicate designs are indispensable to create safe, healthy and comfortable courtyard environment.

The current study developed a numerical strategy to optimize physical environments in courtyard, including distributions of air velocity, airborne pollutant, drought sensation and infection risk. Experimental data from literature was used to validate the numerical models. The influences of courtyard width (D), building height (H), opening status of door were investigated by numerical simulation. Based on the modeled results of drought sensation and infection risk, optimal architectural design strategy was provided to create healthy courtyard environment from the perspectives of pollution mitigation and infectious disease control.

2. Methodology

This section describes the methodologies, which were used to investigate the influences of courtyard dwellings design on physical environment in courtyard. Before conducting numerical cases of courtyard dwellings, validation case with experimental data from available literature was simulated to ensure the reliability. Firstly, the geometric designs of courtyard dwellings were introduced. The geometry of validation case was also illustrated. Next, the numerical models utilized to compute the wind/pollutant distributions were described, including turbulence model, meshing method, boundary condition, computational domain et al. Lastly, the evaluation indexes were shown, including draft sensation, airborne pollution exposure risk etc. Finally, case setups in the current numerical investigation were summarized.

2.1. Geometric designs

Based on surveying and mapping a large number of courtyards dwellings with different scales in Tongli (locating in Jiangsu Province, China) (Wang, 2014), typical prototype of courtyards was summarized and selected in the current numerical study, as shown in Fig. 1. The courtyard was surrounded by two residential buildings and walls. The essential geometric-design factors were described in Fig. 1: width of building (W), width of courtyard (D), height of building (H), thickness of wall (T), length of courtyard (L), width of courtyard door (D_W), height of courtyard door (D_H). The roof slope was fixed as 30°. This current study investigated the influences of geometric-design factors on wind environment and pollutant dispersion in courtyard. Detailed information of case setup was summarized in “2.4 Case setup”.

In order to validate the numerical models, experimental cases from previous study were conducted (Santiago, Martilli, & Martín, 2007). In the validation case, its configuration was formed by a three-dimensional array of cubes: 7 cubes in the stream-wise direction (X axis) and 11 cubes in the span-wise direction (Y axis), as shown in Fig. 2. This validation case was designed to simulate and understand the physical mechanisms responsible for wind environment/pollutant dispersion in urban areas (Santiago et al., 2007). Due to its symmetrical characteristics, only one cube was simulated in the Y-direction. The cube edge length was $H = 0.15$ m. The face-to-face spacing in the stream-wise or span-wise directions was also H. This configuration of cubes in numerical case corresponded to the experiments performed in literature (Brown, Lawson, DeCroix, & Lee, 2001). In Fig. 2, the dotted lines represented locations of measurement sensors. Except for geometries, numerical strategies and settings in the validation case and courtyard case were the same.

2.2. CFD models

For all the numerical cases in the current research, a commercial program ANSYS Fluent 16.0 was used to conduct numerical simulations. This numerical platform is widely adopted in built environment simulations (Chen, Feng, & Cao, 2019). The Reynolds-averaged Navier-Stokes (RANS) equations with a realizable k-ε turbulence model (Blocken & Persoon, 2009; Shih, Liou, Shabbir, Yang, & Zhu, 1995) was adopted to solve turbulent wind flow in computational domain. Based on the previous literature focusing on outdoor wind environment simulation (Liu et al., 2018), the realizable k-ε turbulence model could provide satisfied results with relative errors lower than 15 % compared with experimental data. Some advanced turbulence models (such as LES, Large Eddy Simulation) are proven to be able to generate more accurate results in outdoor simulations (Blocken, 2018). However, the computation cost is considerate and not suitable for engineering application. Based on the trade-off between model accuracy and computing cost, the RANS models are recommended in engineering design for outdoor simulations (Liu et al., 2018). The finite volume method (FVM) was used to solve governing transport equations, including mass conservation, mean velocity, turbulence quantities and airborne pollutant. PISO algorithm was used for pressure and velocity coupling, and first-order discretization schemes were used for solving all the independent variables.

To simulate airborne pollutant (such as SARS-CoV-2) distributions in courtyard environment, species-transport equation was solved, as described by formula (1). The droplets exhaled by human contain virus, forming one of the main sources of airborne disease. For fine particles (or droplets) with relatively small size, they follow air flow patterns and transport due to air drag force. For coarse particles with relatively large size, they deviate from air streamlines and deposit on different surfaces (e.g. ground, facilities, human body). In the current simulations, it was assumed that the proper social-distance was kept. Therefore, only air transmission of fine particles were considered in infection risk assessment in the current study. For airborne pollutant simulation, because the mean diameter of the droplets exhaled by breathing was 0.4 μm (Gupta, Lin, & Chen, 2010), the effect of gravitational settling on droplet dispersion was negligible (Zhao, Chen, & Tan, 2009). Furthermore, previous researches have indicated that the transient process from a droplet to a droplet nucleus due to evaporation is also negligible for particles with a diameter of 0.4 μm (Chen & Zhao, 2010). Thus, modeling the exhaled droplets as gaseous contaminants is reasonable in engineering application (Chen et al., 2014). The “User-Defined-Scalar (UDS)” was used to simulate air pollutant motion in ANSYS-FLUENT.

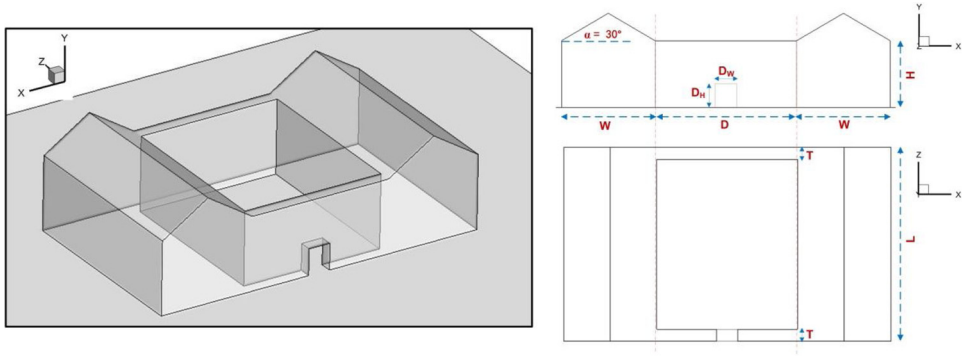

Fig. 1. The geometries of courtyards dwellings in the current numerical study.

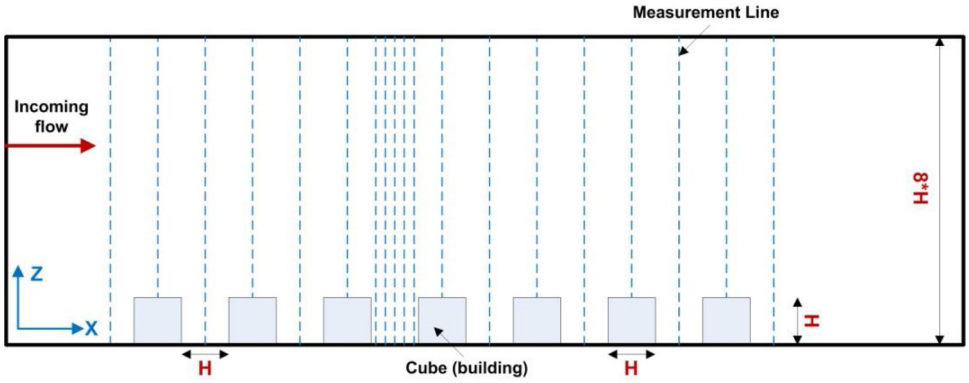

Fig. 2. The geometries of validation case in the current numerical study.

$$\frac{\partial(\rho C)}{\partial t} + \frac{\partial}{\partial x_i}(\rho u_i C - \Gamma \frac{\partial C}{\partial x_i}) = S_c \quad (1)$$

where t is the physical time (s), C is the particle/virus concentration (#/m^3), ρ is the density of air (kg/m^3), x_i (i = 1, 2, 3) are the three spatial coordinates (m), u_i is the averaged air velocity components in the three dimensions (m/s), Γ is the effective particle diffusivity (Pa*s), and S_c is the particle source term. The effective particle diffusivity has the following form:

$$\Gamma = \rho(D + \nu_p) = \rho(D + \nu_t) \quad (2)$$

where D is the Brownian diffusivity of particles (m^2/s), ν_p is the particle turbulent diffusion coefficient ((m^2/s), equaling to the air turbulence viscosity ν_t according to Zhao et al., 2009). In the User-Defined-Scalar (UDS) equation, particle size was considered in determination process of Brownian diffusivity (Zhao et al., 2009). Based on the previous literature on diameter of droplet nuclei (Ai, Mak, Gao, & Niu, 2020), the size of respiratory droplet nucleus was set as 1 μm in the current numerical simulation.

In order to properly simulate wind environment and airborne pollutant dispersion in courtyard, an external domain around the target courtyard dwelling was formed, as shown in Fig. 3. Although geometric-design factors of courtyard dwellings varied in different cases, the external domain sizes were fixed. In Fig. 3, the geometric factors are: X1 (17 m), X2 (62 m), Y1 (10 m), Z1 (17 m). We have tested different domain sizes (0.2–2 times of the domain sizes in the current research), and the domain in Fig. 3 was large enough for modeling physical environment in courtyard. It is unnecessary to continue to increase the simulation domain. Due to the relatively low simulation-efficiency of the trial-error method, we will develop an adaptive method to automatically determine domain sizes for courtyard environment modeling in our future study.

The platform GAMBIT 2.4.6 was adopted to generate grids in computational domain. The truncation errors of hexahedral meshes are lower than those of tetrahedral mesh. Therefore, hexahedral meshes were generated for discretizing the governing transport equations. In order to obtain high quality mesh, the whole computational domain was divided into dozens of sub-regions. Almost 90 % of mesh elements had skewness values lower than 0.1. The maximum grid size was about 2 m near the boundary of computational domain, and it was gradually reduced to 0.2 m near the courtyard dwellings. For the inner zone of courtyard environment, the grid resolution was refined to 0.1 − 0.2 m. The total grid number was about 1.5–2.2 million for cases with different configurations of courtyard dwellings. In case 2, the grid number was about 1.8 million. Different grid numbers (1.0/1.8/2.5 million) with the same meshing strategy were tested, and the numerical results indicated that grid number of 1.8 million was enough. Similar mesh independent study was conducted in different courtyard cases.

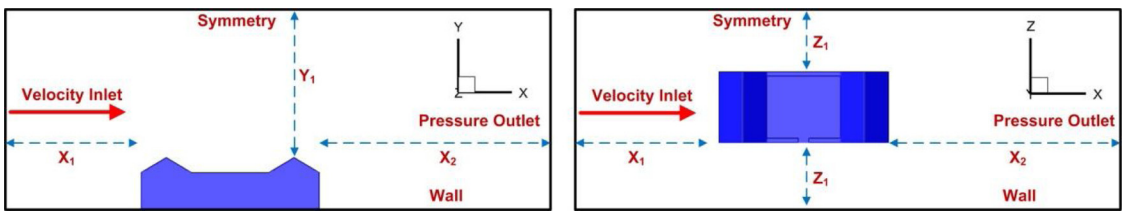

Fig. 3. The geometries of computational domain in numerical study.

For boundary conditions of computational domain, the upstream left surface was set as "velocity Inlet", as shown in Fig. 3. The top surface was set as "Symmetry" (Liu et al., 2018). The ground and walls of courtyard dwelling were set as "Wall". Other boundary surfaces were set as "Pressure Outlet". The vertical velocity profile for the inflow boundary was modeled as a power law, and the vertical profiles for k_z and ε_z was taking from previous study (Richards & Hoxey, 1993). The detailed information about inflow boundary conditions could be found in literature (Liu et al., 2018).

$$U_Z = U_r(z/z_r)^{\alpha} \tag{3}$$

$$k_z = U_{ABL}/\sqrt{C_\mu} \tag{4}$$

$$\varepsilon_z = U_{ABL}/(k(z + z_0)) \tag{5}$$

Where Z is height (m), U_r is velocity (m/s) at reference height, Z_r is reference height (m), k is the Karman constant (0.4), α is constant (0.3). U_{ABL} is the atmospheric boundary layer friction velocity (m/s), and how to determine friction velocity was illustrated in previous study (Liu et al., 2018). In Case 2–7, U_r and Z_r were set as 2.6 m/s and 3 m, respectively.

In this study, a point pollution source was set in the middle position of courtyard to simulate generation of airborne droplets, as described by Fig. 4. The point pollutant source was located at the height of 1.6 m. The air pollutant concentration was set as zero at the inflow boundary. The air velocity, *PD* index (percent dissatisfied due to draft) and air pollutant concentration were quantitatively evaluated in the target zone of courtyard, as shown by dashed box in Fig. 4. The target zone represents the major area of human activity, where the point pollution source was located. The height and length of the target zone were 2 m and 12 m, respectively. The width (D_x) of the target zone varied in different cases, and was summarized in the following part. Based on previous study (Buonanno, Stabile, & Morawsk, 2020), the source strength (droplet generation rate) was set as "1200 (quantum/h)", which was defined as high quanta emission rate. The respiratory viral load emitted is expressed in terms of quanta emission rate (quantum/h), and a quantum is defined as the dose of airborne droplet nuclei required to cause infection in 63 % of susceptible persons (Buonanno et al., 2020). In the previous study (Buonanno et al., 2020), low (< 1 quantum/h) and high (> 100 quantum/h) quanta emissions were also defined. From the perspectives of engineering safety, a high quanta emission rate (1200 quantum/h) was considered in the current research, which corresponds to extremely high RNA copes (1E + 11 copies/mL). It is assumed that the effect of airborne pollutants on air flow is negligible, while airflow field and turbulence characteristics determine pollutant distributions.

2.3. Evaluation index

The following indexes were adopted to evaluate physical environment in courtyard: air velocity magnitude, draft sensation and airborne pollutant concentration. Draft sensation is related to human comfort, and air pollution concentration represents exposure to exhaled droplets (Zhai, Xue, & Chen, 2014). Draft is an undesired local cooling of human body caused by air movement, and has been identified as one of the most annoying factors during the cooling. *PD* (percent dissatisfied due to draft) represents percentage of the population feeling draft when exposed to a given mean velocity. Eq. (6) was used to calculate *PD* index, which was based on distributions of turbulent air velocity. For air velocity, *PD* index and airborne pollutant concentration, the maximum, average and minimum values in the target zone were calculated to compare and evaluate different cases.

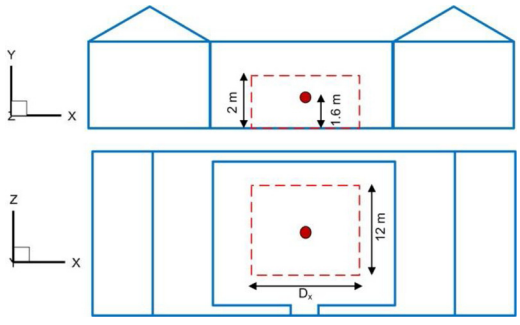

Fig. 4. The position of airborne pollution source and target zone in courtyard.

$$PD = (34 - t_a)*\max(0.05, (V - 0.05))^{0.62}(0.37*V*Tu + 3.14) \tag{6}$$

Where t_a is air temperature (℃), V is air velocity (m/s), Tu is turbulence intensity. If the calculated *PD* is higher than 100 %, the model assumes that practical *PD* value equals to 100 %. The isothermal conditions were simulated in all the cases in the current study. The V and Tu were determined by numerical modeling results, and t_a was assumed as constant value (25 ℃).

To determine infection risk/possibility (R, %), the well-known Wells-Riley equation was utilized, as described by Eq. (7). This quantitative index has been widely used in medical surveys (e.g. SARS, SARS-CoV-2) (Buonanno et al., 2020). In the current numerical study, the activity time (exposure time, T) was assumed as one hour. In courtyard, the point source described above represented one infected patient, who generated droplets containing virus through breathing or talk. The R value with exposure time of one hour was adopted to assess infection possibility of different spatial locations in courtyard environment.

$$R = (1 - \exp(-IR* \int_0^T n(t)dt))*100 \tag{7}$$

Where R is infection risk/possibility (%), t is physical time (h), T is total exposure time (h), IR is inhalation rate of exposed subject (m^3/h), n(t) is air pollutant concentration (quantum/m^3). The exposed subjects/occupants were assumed to stand or perform normal exercise, and the IR value was 0.96 (m^3/h) (Buonanno et al., 2020).

The solutions might be considered to be converged when the sum of the normalized residuals for all the cells became less than 10^{-12} for UDS and 10^{-3} for all other variables. Besides, we have monitored air velocity/UDS values at seven points in numerical iterations. Another criterion was that the monitored air velocity magnitude/UDS kept steady.

2.4. Case setup

Table 1 introduces cases setup in the current numerical study. Case 1 was set for model validation, and the detailed information about experiments could be found in literature (Brown et al., 2001). Case 2 was set as benchmark case, which was compared with Case 3−7. Case 3–4 were conducted to investigate the influences of courtyard width (D) on wind environment and pollutant dispersion. Case 5 was set to determine the effects of courtyard dwelling height on wind environment. Case 6–7 were set to compare situations with different door opening status. The heights of "2.8 m" and "5.6 m" represent buildings with one-

Table 1
Detailed information of Case setup.

Case No.	D (m)	H (m)	D_x (m)	Door status
1	N	N	N	N
2	11.8	5.6	10.8	One-side opening
3	5.8	5.6	4.8	One-side opening
4	16.8	5.6	15.8	One-side opening
5	11.8	2.8	10.8	One-side opening
6	11.8	5.6	10.8	Two-sides opening
7	11.8	5.6	10.8	Two-sides closed

floor and two-floor, respectively. In cases 2–7, the following geometric-design factors were set as fixed values: width of building (W, 7.8 m), thickness of wall (T, 1 m), length of courtyard (L, 16 m), width of courtyard door (D_W, 1.8 m), height of courtyard door (D_H, 2 m).

The flow patterns of validation case and courtyard case were similar, including atmospheric free-flow, vortex flow near wall surfaces, et al. There are no available wind tunnel results for courtyard environment. In future, we will conduct accurate and reliable wind tunnel experiments for courtyard architecture.

3. Results

The results section was organized as follow: numerical model validation (Case 1), the influences of courtyard width (Case 2–4), the influences of building height (Case 5), the influences of door status (Case 6–7). In each case, spatial distributions of wind environment, airborne pollutant, drought sensation and infection risk were quantitatively analyzed.

3.1. Case 1: model validation

Fig. 5 shows the numerically simulated and measured velocity results in Case 1. Detail information about the wind tunnel experiments could be found in literature (Brown et al., 2001). A reference velocity of U_{ref} (constant: 3 m/s) was used to present variables in a normalized form. Vertical profiles of normalized mean stream-wise velocity and vertical velocity were compared. For stream-wise velocities, predicted and experimental results agreed well, and normalized mean square error (NMSE) was lower than 0.02. For vertical velocities, the NMSE value (0.25) was higher than that of stream-wise velocities. Previous numerical study also performed the same wind tunnel case and obtained the similar error levels (Santiago et al., 2007). The validated numerical strategy was used in courtyard cases to investigate the influences of architectural design parameters on wind environment and airborne pollutant exposure.

For this validation case, statistic analysis was also conducted to quantitatively characterize the numerical results. Normalized mean square error (*NMSE*) and correlation coefficient (*CR*) were computed. The *NMSE* indicates a value of normalized discrepancies between the simulated and experimental values, and *CR* indicates the relevancy between these two series of data. Eqs. (8 and 9) described the accurate definition of *NMSE* and *CR*. Table 2 shows the computed results of *NMSE* and *CR*. The *CR* was particularly high, showing that the numerical model was able to correctly reproduce the profiles of experimental data (Table 2).

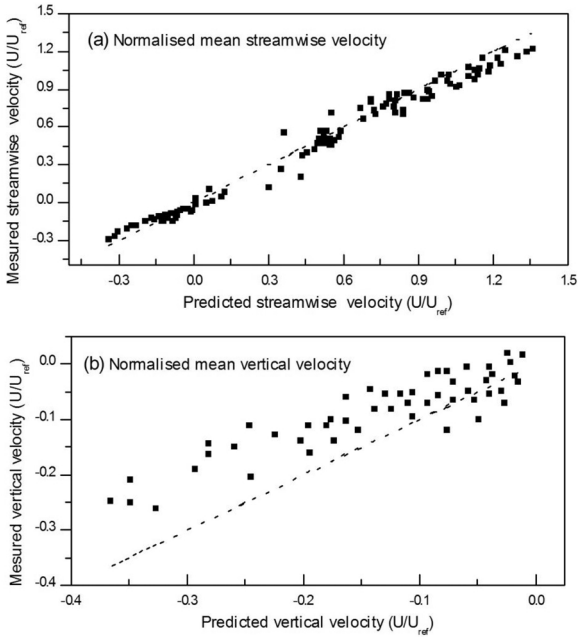

Fig. 5. Comparison of experimental and simulated results of velocities in case 1: (a) stream-wise velocity (U/U_{ref}), (b) vertical velocity (U/U_{ref}).

Table 2
Computed results of *NMSE* and *CR*.

	NMSE	*CR*
Stream-wise Velocity	0.013	0.990
Vertical Velocity	0.251	0.921

$$NMSE = \frac{\sum (O_i - P_i)^2}{\sum (O_i P_i)} \quad (8)$$

$$CR = \frac{\sum (O_i - O)(P -_i P)}{[\sum (O_i - O)^2]^{1/2}[\sum (P_i - P)^2]^{1/2}} \quad (9)$$

Where O_i and P_i are measured and simulated velocity (m/s) values for a certain point (i), respectively. O and P are measured and simulated average velocity (m/s) value for all the points, respectively.

3.2. Case 2–4: the influences of courtyard width

Fig. 6 shows the numerically simulated results of dimensionless velocity magnitude (V/V_0) and streamlines in case 2 with courtyard width of 11.8 m. Physical environments in two vertical planes (XY plane, Z= ± 2 m) were analyzed. In Case 2–7, the reference velocity magnitude (V_0) was set as 1.4 m/s. In the courtyard, velocity distribution (V/V_0) was non-uniform, ranging from 0.02 to 0.6. Tow big vortexes formed near building roof, as shown in Fig. 6(b1-b2). In the target zone, the average and maximum velocity magnitudes were 0.42 m/s and 1.31 m/s, respectively. The semi-enclosed structure of courtyard generated complex velocity field, including obvious vortexes and non-uniformity. The vortexes may negatively influence air pollutant dispersion, and relatively high air velocity may cause draught sensation.

Fig. 7 shows the numerically simulated results of dimensionless airborne pollutant concentration (C/C_0) and *PD* index in case 2. The reference pollutant concentration (C_0) was set as 6.67E-04 (quantum/m^3). Airborne pollutant concentrations near the upstream building were much higher than those in other regions. Turbulent diffusion and complex vortex structure caused the non-uniform distribution of air pollutant. Occupants in rooms of the upstream building may suffer from serious airborne pollution, due to natural ventilation or envelope infiltration (Ng et al., 2019; Qi, Cheng, Katal, Wang, & Athienitis, 2019). In courtyard environment, outdoor spaces near the upstream building should be controlled by some artificial measures (e.g. air cleaning device) (Boppana, Wise, Ooi, Zhmayev, & Poh, 2019). Similarly, *PD* distributions were non-uniform, ranging from 0 % to 53 %. In previous literature, design objective is to control average *PD* to be below 15 % (Zhai et al., 2014). In the target zone of courtyard, the average and maximum *PD* values were 24 % and 53 %, which were higher than design objective of 24 %. In practical conditions, layout of occupant activity facilities (e.g. tea table, chair and fitness equipment) should also be properly designed to reduce pollutant exposure and draught sensation.

Fig. 8 shows the numerically simulated results of dimensionless air pollutant concentration (C/C_0) and *PD* index in Case 3 with relatively smaller courtyard size. In Case 3, courtyard width was 5.8 m, while it was 11.8 m in Case 2. Air pollutant concentrations in narrow courtyard of Case 3 were higher than those in Case 2. More air pollutants accumulated in narrow space, leading to more serious pollutant exposure. The *PD* values in Case 3 were smaller than those in Case 2. In the target

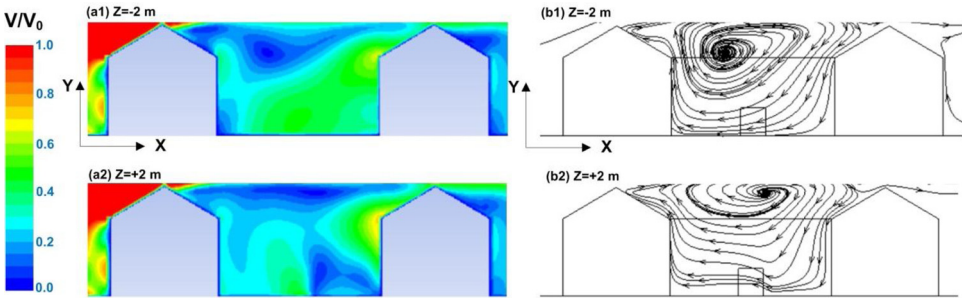

Fig. 6. Simulated results of dimensionless velocity magnitude (V/V_0) and streamlines in case 2: (a1) distributions of (V/V_0) in Z-plane (Z = −2 m); (a2) distributions of (V/V_0) in Z-plane (Z = +2 m); (b1) distributions of streamlines in Z-plane (Z = −2 m); (b2) distributions of streamlines in Z-plane (Z = +2 m).

zone of Case 3, the average and maximum *PD* values were 18 % and 53 %, respectively. Lower air velocities in narrow space will relieve draught sensation.

Fig. 9 shows the numerically simulated results of dimensionless air pollutant concentration (C/C_0) and *PD* index in Case 4 with largest courtyard. In Case 4, courtyard width was 16.8 m, while it was 11.8 m in Case 2. Similar to results in Fig. 7, air pollutant concentrations near the upstream buildings were higher than other regions. Airborne pollutant concentrations in Case 4 were lower than those in Case 2–3. In the target zone of Case 4, the average and maximum *PD* values were 31 % and 50 %, respectively. In Case 4, higher air velocities in wide courtyard space caused more serious drought sensation and lower air pollution exposure.

Fig. 10 quantitatively analyzes the influences of courtyard width (*D*) on wind environment and air pollutant dispersion. Courtyard width plays an important role in airborne pollutant distributions. When *D* value increased (from 5.8 m to 11.8 m), average air pollutant concentration decreased by 80 %. Narrow courtyard space is not beneficial for human health. Courtyard width and average *PD* value in the target zone was positively correlated. The average velocity magnitudes in Case 2–4 were 0.42 m/s, 0.31 m/s and 0.62 m/s, respectively. In large courtyard space, higher velocity magnitude will intensify drought sensation. Overall, width of courtyard (*D*) is a very essential parameter in architectural and landscape design, from the perspectives of physical environment.

Fig. 11 quantitatively analyzes the influences of courtyard width (*D*) on infection risk (*R*, %) in Case 2–4. This index indicates infection possibility in the courtyard environment with one infectious patient. The *R* value is positively correlated with airborne pollutant concentration, as described by Eq. (7). Increase of courtyard width could reduce infection risk. The maximum *R* values in Case 2–4 were 0.3 %, 1.0 % and 0.2 %, respectively. In Case 2 and Case 4 with relatively longer courtyard width, infection possibility values were higher in regions locating upstream of infectious occupant, which was quite similar to air pollutant distributions. When *D* value varied from 5.8 m to 11.8 m, infection risk index decreased significantly. Large courtyard space led to better natural ventilation performance and pollutant removal effect. In previous study (Buonanno et al., 2020), the *R* values in typical natural-ventilated rooms (pharmacy, supermarket, post office, bank) were from 2.19 to 3.70 before lockdown during the COVID-19 period. Compared to the *R* values in indoor environments, the courtyard environments in Case 2–4 were relatively safe. The "social-safe distance" from infectious patient (air pollutant source in numerical cases) could be defined as these with *R* value lower that 0.1 %. Based on numerical results, it was concluded that the safe distance of 3 m was enough for occupants in courtyard environment.

3.3. Case 5: the influences of building height

Fig. 12 shows the numerically simulated distributions of dimensionless air pollutant concentration and *PD* values in Case 5. Building height in this case was 2.8 m (one-floor), and other geometric design parameters were the same to Case 2 (two-floor). Airborne pollutant distributions were quite similar to that in Case 2, in which pollutant concentrations near building roof were higher than other regions. The drought sensation level was slightly lower than Case 2. The average velocity of target zone in Case 5 was 0.46 m/s, while in Case 2 it is 0.42 m/s. In the target zone of Case 5, the average and maximum *PD* values were 25 % and 50 %, respectively. The infection risk distributions in Case 5 were quite similar to that in Case 2, and the maximum *R* value was lower than 0.3.

Fig. 13 quantitatively compares the average dimensionless air pollutant concentrations and *PD* values of the target zone in Case 2 and Case 5. When building height decreased from 5.6 m to 2.8 m, average (C/C_0) decreased by 18 %. In courtyards with lower building height, air pollutants generated in courtyard moved out more easily. Similarly, the maximum (C/C_0) value in Case 5 was slightly lower than this in Case 2. The average *PD* value in the target zone increased by 7 % when building height decreased from 5.6 m to 2.8 m. Compared with courtyard width, the effects of building height on wind environment and air pollutant distribution are less critical.

3.4. Case 6–7: the influences of door status

This current research also investigated the influences of door status on wind environment and airborne pollutant distributions in courtyard,

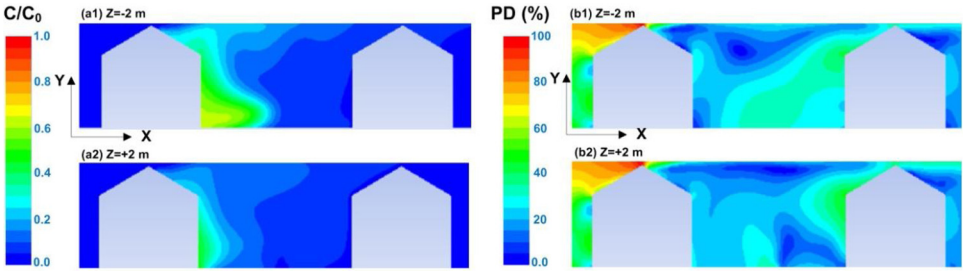

Fig. 7. Simulated results of dimensionless pollutant concentration and *PD* index in case 2:(a1) distributions of (C/C_0) in Z-plane (Z = −2 m); (a2) distributions of (C/C_0) in Z-plane (Z = +2 m); (b1) distributions of *PD* in Z-plane (Z = −2 m); (b2) distributions of *PD* in Z-plane (Z = +2 m).

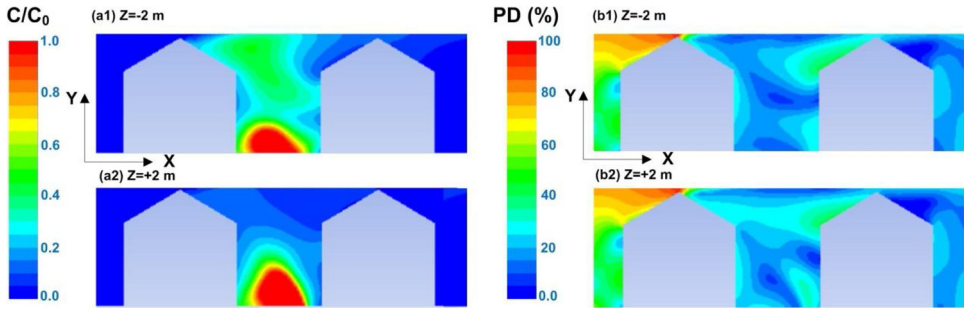

Fig. 8. Simulated results of dimensionless pollutant concentration and *PD* index in case 3:(a1) distributions of (C/C_0) in Z-plane (Z= −2 m); (a2) distributions of (C/C_0) in Z-plane (Z= +2 m); (b1) distributions of *PD* in Z-plane (Z= −2 m); (b2) distributions of *PD* in Z-plane (Z= +2 m).

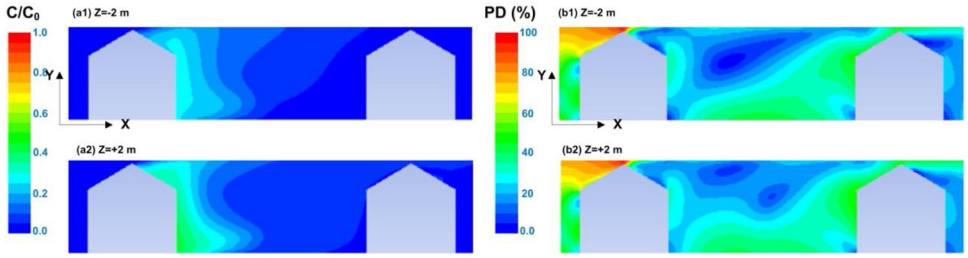

Fig. 9. Simulated results of dimensionless pollutant concentration and *PD* index in case 4:(a1) distributions of (C/C_0) in Z-plane (Z= −2 m); (a2) distributions of (C/C_0) in Z-plane (Z= +2 m); (b1) distributions of *PD* in Z-plane (Z= −2 m); (b2) distributions of *PD* in Z-plane (Z= +2 m).

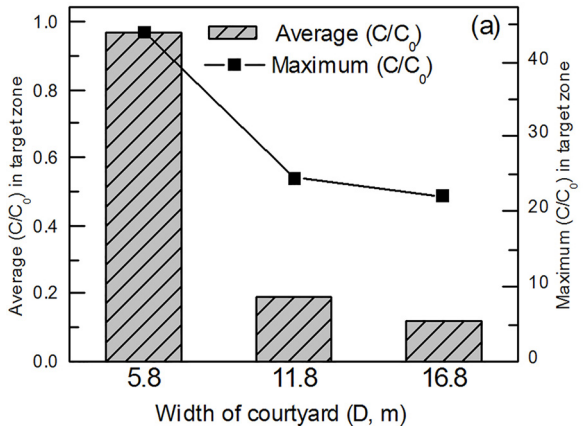

Fig. 10. Influences of width of courtyard (D) on dimensionless pollutant concentration and *PD* in target zone.

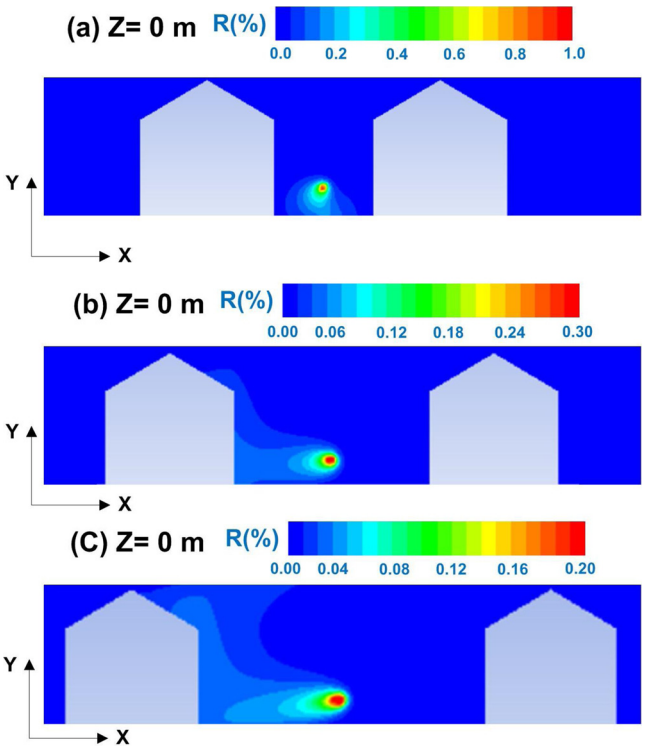

Fig. 11. Simulated infection risk in cases with different courtyard width: (a) Case 3, (b) Case 2, (c) Case 4.

as shown in Fig. 14. In Case 2 described above, only one-side door was open. Two-side doors were open in Case 6, and doors were completely closed in Case 7. The detailed door sizes in Case 6–7 were the same to Case 2. The architecture designs of Case 6–7 were the same to that in Case 2, except for door opening status.

Figs. 15 and 16 show the simulated dimensionless air pollutant concentrations and *PD* values in Case 6 and Case 7, respectively. For airborne pollutant field, pollutant concentrations near the upstream buildings were higher in all the cases with different door opening statuses (Case 2, 6, 7). If door opening level decreased (from "two-sides opening" to "one-side opening", and to "two-sides closed"), the polluted area with (C/C_0) value higher than 0.1 increased. For *PD* distributions, the non-uniformity was very obvious, ranging from lower that 1 %–50 %. In the upper zone (about 2 m in Y-direction), the *PD* values were quite low due to the formation of big vortexes in Case 6–7. The *R* values were positively correlated with air pollutant field. Infection risk distributions in Case 6–7 were quite similar to those in Case 2, because of the similar distributions of (C/C_0).

Fig. 17 quantitatively describes the influences of door opening status on dimensionless air pollutant concentrations and *PD* values in the target zone of Case 6–7. The differences of average (C/C_0) and *PD* values were not obvious among the three cases. Once the door status was changed, turbulence characteristics and vortex structures varied complicatedly, resulting in different air pollutant distributions. In the current research, incoming air flow direction (as shown by Fig. 2) was parallel to the door surface. Therefore, the influences of door opening status were not significant. If the incoming flow direction is vertical to

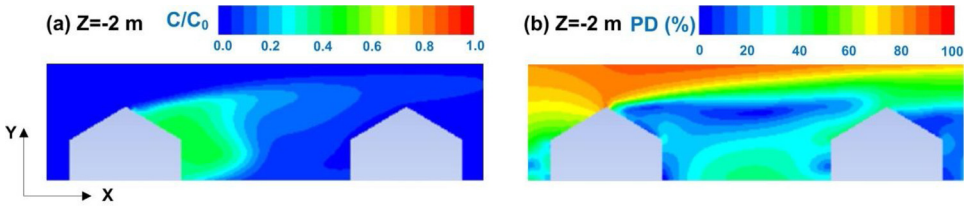

Fig. 12. Simulated results of dimensionless pollutant concentration and *PD* index in case 5: (a) distributions of (C/C_0) in Z-plane (Z = −2 m); (b) distributions of *PD* in Z-plane (Z = −2 m).

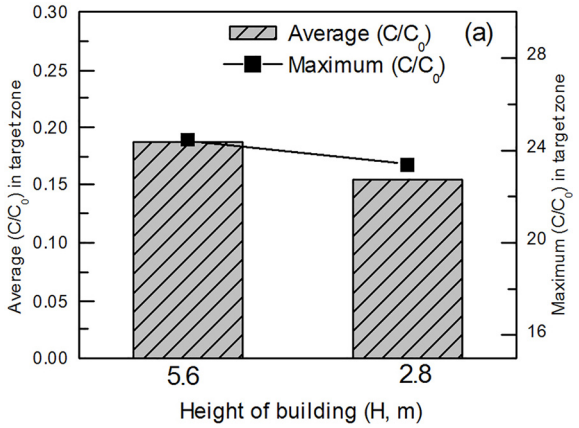

Fig. 13. Influences of height of building (H) on dimensionless pollutant concentration and *PD* in target zone.

door surfaces, the role of door opening status may be essential, and doors are commonly to be closed to avoid serious drought sensation in courtyard environment. In our future work, numerical cases with different incoming flow directions will be conducted to provide more detailed design suggestions.

4. Discussions

4.1. Infection risk in static wind conditions

In Case 2–7 described above, simulated velocity magnitudes in courtyard environment were relatively high: the average and maximum velocities were 0.4 − 0.6 m/s and 0.7–1.3 m/s, respectively. Strong air convection intensified air pollutant dispersion and escape out of courtyard. In static wind conditions with extremely low air velocities, air pollutants may accumulate in courtyard, resulting in high infection risk. Fig. 18 shows the simulated distributions of *R* values in Case 2–3 under static wind conditions. In static wind cases, U_r and Z_r in Eq. (3) were set as 0.05 m/s and 3 m, respectively. Weak air motion led to high infection risk obviously. For example, the *R* values in Case 3 (static wind) were about 3 times of that in non-static wind case. In static wind conditions, infection risks in courtyard were comparable to those in rooms during the COVID-19 period (Buonanno et al., 2020). Therefore, the courtyard environment was not always safe for occupants, especially in static wind conditions. Based on indoor environment control strategies, some artificial measures (e.g. ventilator and purifier applied in outdoor) could be considered to create healthy courtyard environment.

4.2. Limitations and future studies

Optimal design of courtyard environment is a complex and systematic task, including multiple objectives and design parameters. The main design objectives are space utilization, thermal comfort, daylighting, airborne disease control et al. The design parameters include climate characteristics, orientation, geometry, construction materials, landscape and vegetation arrangements (Hong & Lin, 2015). The interaction between indoor and courtyard environments, and the influence of surroundings on courtyard should also be taken into consideration in design process (Liu et al., 2018; Wang, Karava, & Chen, 2015). Due to its complexity, the multi-objective optimization needs series of CFD cases and considerate computing effort. The current research conducted optimal design of courtyard with limited number of cases. Although the numerical results could provide critical support for engineering application, the optimization potential and computing speed are not satisfied. To fulfill the complex design and optimization task, coupling CFD simulations and machine learning (ML)/artificial intelligence (AI) is a feasible solution. ML/AI method could rapidly finish multi-objective optimization process by using simulated results from limited cases (Ren C. & Cao, 2020; Ren J. & Cao, 2020). CFD + MA/AI are effective methods for reducing CFD simulation efforts, and are very popular in indoor environment control (Feng, Yu, & Cao, 2019). With the development of ML/AI, coupling the advanced techniques into outdoor environment design is becoming more and more promising.

In order to create healthy and comfortable courtyard environment for humans, the geometric parameters (courtyard width, building height and door opening status) should be paid attentions in architectural design, especially for the determination of courtyard width. Due to the semi-enclosed characteristics of courtyard, complex turbulent airflow field and vortexes were generated, leading to air pollution accumulation in the courtyard. It is impossible to completely avoid person-to-person pollutant exposure (e.g. droplets transport under static wind condition during the COVID-19 period) only relying on passive architectural design. Therefore, some artificial measures (e.g. outdoor ventilator, air cleaning device) should be adopted to remove air pollutant rapidly. Previous studies have proven that outdoor air cleaning devices were very effective to control air quality in community environment (Buonanno et al., 2020). In future research, we will investigate how to apply advanced air cleaning devices in courtyard environment control (Feng, Yang, & Zhang, 2020), and develop some

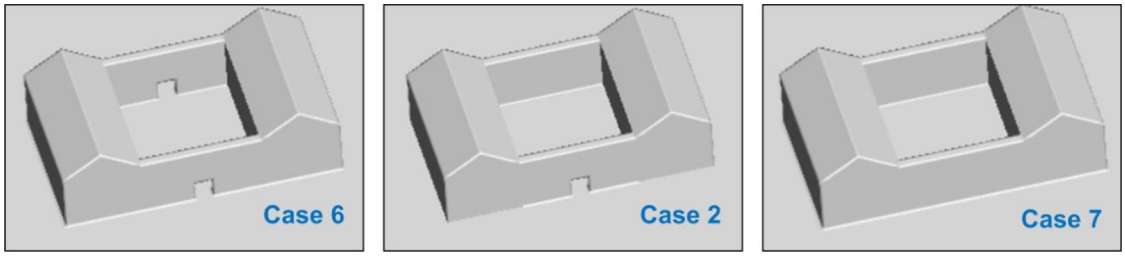

Fig. 14. Door opening status in Case 2, 6 and 7.

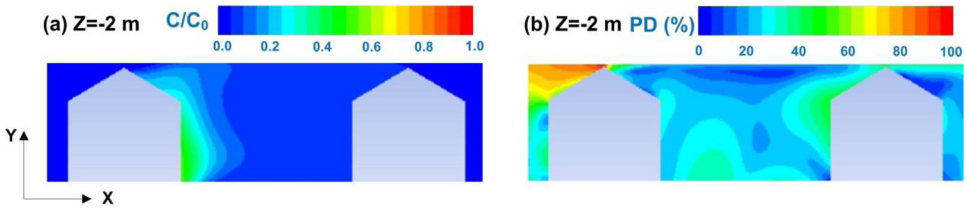

Fig. 15. Simulated results of dimensionless pollutant concentration and *PD* index in case 6: (a) distributions of (C/C_0) in Z-plane (Z = −2 m); (b) distributions of *PD* in Z-plane (Z = −2 m).

intelligent control strategy adaptive to changes of climate conditions and human behavior (Cao & Ren, 2018; Ren & Cao, 2019).

Courtyard is typical semi-enclosed space, which is different from the fully enclosed (indoor) and open (outdoor) environments. In enclosed space, the effective methods for airborne disease control include utilization of building device (e.g. increase ventilation rate by fan) and keeping proper social-distance (Chia et al., 2020; Xu & Liu, 2018). In open space, the main method for airborne disease control is keeping social-distance (Buonanno et al., 2020). For courtyard environment, all the control methods could be considered, including using portable ventilation/filtration device, keeping proper social-distance and optimal architecture design. In future study, we will investigate how to couple all the disease control methods in courtyard design/operation periods, to effectively lower infection risk and economic cost.

In this current study, the *PD* index was adopted to evaluate drought sensation in courtyard environment. However, this quantitative index was developed for indoor environment (Zhai et al., 2014). There is no available drought sensation index for outdoor environment evaluation. Actually, the semi-enclosed courtyard is a transitional region between indoor and outdoor environments. Therefore, it is necessary to develop suitable drought sensation indexes to properly assess different types of built environments (e.g. indoor/outdoor/transitional regions).

5. Conclusions

This current study developed a numerical strategy to investigate the influences of geometric design parameters on wind environment, air pollutant distribution and infection risk in courtyard. Air pollution source in courtyard was set to simulate droplets production of human breathing. The realizable *k-ε* turbulence model was adopted, and experimental results from literature were used to validate the numerical model. Based on the results, the following conclusions can be drawn:

(1) The width of courtyard (*D*) is the most essential design parameter for drought sensation and infection risk in courtyard. If *D* value varied from 5.8 m to 11.8 m, average air pollutant concentration decreased by 80 %. Other geometric design parameters (building height, door status) also have obvious influences on air pollutant concentration, but not as significant as the width of courtyard.
(2) In static wind conditions, infection risk increased significantly. Infection possibility (with *R* value up to 3 %, static wind conditions) in courtyard was comparable to those in indoor environments during the COVID-19 period. In non-static wind conditions, courtyard environment was relatively safe with *R* values lower than 1 %.
(3) Optimal architectural design could improve air quality and safety in courtyard. However, it is of great difficulty to avoid person-to-person pollutant exposure (e.g. droplets transport in COVID-19 period) only relying on passive design in complex climates. Some artificial measures (e.g. outdoor ventilator, air cleaning device) should be adopted in courtyard environment to remove air pollutant rapidly and ensure personnel safety.

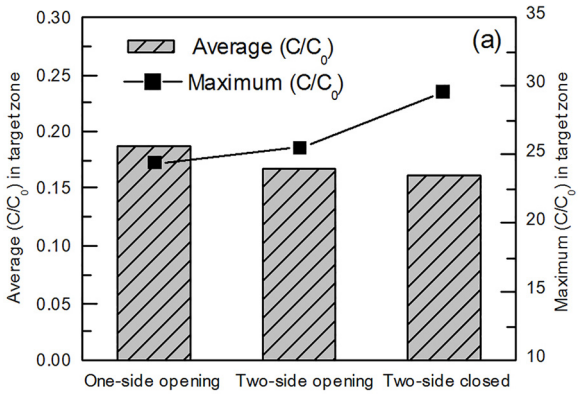

Fig. 17. Influences of status of doors on dimensionless pollutant concentration and *PD* in target zone.

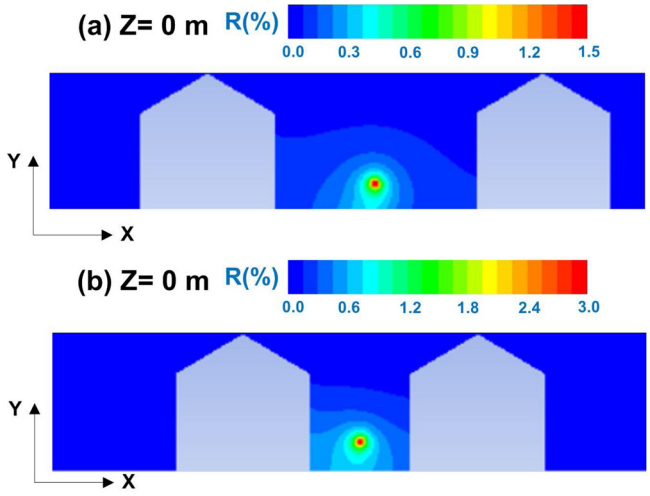

Fig. 18. Simulated infection risk in cases under static wind conditions: (a) Case 2, (b) Case 3.

Declaration of Competing Interest

The author(s) declared no potential conflicts of interest with respect to the research, authorship, and/or publication of this article.

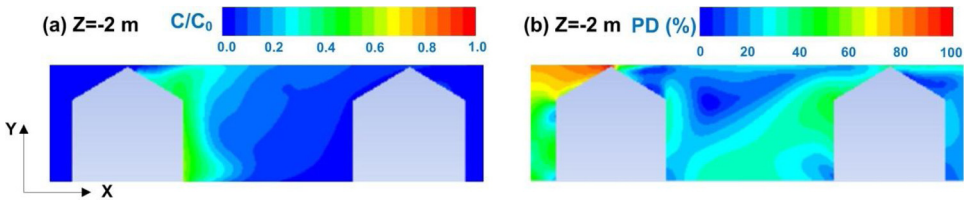

Fig. 16. Simulated results of dimensionless pollutant concentration and *PD* index in case 7: (a) distributions of (C/C_0) in Z-plane (Z = −2 m); (b) distributions of *PD* in Z-plane (Z = −2 m).

Acknowledgements

The authors would like to acknowledge the coordinated support from National Key R & D Program of China (Grant Nos. 2016YFC0700200, 2016YFC0700203).

References

Ai, Z., Mak, C., Gao, N., & Niu, J. (2020). GaoTracer gas is a suitable surrogate of exhaled droplet nuclei for studying airborne transmission in the built environment. *Building Simulation, 13*, 489–496.

Blocken, B. (2018). LES over RANS in building simulation for outdoor and indoor applications: A foregone conclusion? *Building Simulation, 11*, 821–870.

Blocken, B., & Persoon, J. (2009). Pedestrian wind comfort around a large football stadium in an urban environment: CFD simulation, validation and application of the new Dutch wind nuisance standard. *Journal of Wind Engineering and Industrial Aerodynamics, 97*, 255–270.

Boppana, V., Wise, D., Ooi, C., Zhmayev, E., & Poh, H. (2019). CFD assessment on particulate matter filters performance in urban areas. *Sustainable Cities and Society, 46*, Article 101376.

Brown, M., Lawson, R., DeCroix, D., & Lee, R. (2001). Comparison of centerline velocity measurements obtained around 2D and 3D buildings arrays in a wind tunnel, Report LA-UR-01-4138, Los Alamos National Laboratory. *Los Alamos Science*.

Buonanno, G., Stabile, L., & Morawsk, L. (2020). Estimation of airborne viral emission: Quanta emission rate of SARS-CoV-2 for infection risk assessment. *Environment International, 141*, Article 105794.

Cao, S. J., & Ren, C. (2018). Ventilation control strategy using low-dimensional linear ventilation models and artificial neural network. *Building and Environment, 144*, 316–333.

Carlos, R., Eduardo, D., Carmen, C., & Victoria, L. (2019). Tempering potential-based evaluation of the courtyard microclimate as a combined function of aspect ratio and outdoor temperature. *Sustainable Cities and Society, 51*, Article 101740.

Chen, C., Zhu, J., Qu, Z., Lin, C.-H., Jiang, Z., & Chen, Q. (2014). Systematic study of person-to-person contaminant transport in mechanically ventilated spaces (RP-1458). *HVAC&R Research, 20*, 80–91.

Chen, H., Feng, Z., & Cao, S. J. (2019). Quantitative investigations on setting parameters of air conditioning (air supply speed and temperature) in ventilated cooling rooms. *Indoor and Built Environment* Accepted.

Chen, C., & Zhao, B. (2010). Some questions on dispersion of human exhaled droplets in ventilation room: Answers from numerical investigation. *Indoor Air, 20*, 95–111.

Chia, P., Coleman, K., Tan, Y., Ong, S., Gum, M., Lau, S., et al. (2020). Detection of air and surface contamination by SARS-CoV-2 in hospital rooms of infected patients. *Nature Communications, 11*, 1–7.

Feng, Z., Yang, J., & Zhang, J. (2020). A numerical optimization on newly developed electrostatic enhanced pleated air filters for efficient removal of airborne ultra-fine particles: Towards sustainable urban and built environment. *Sustainable Cities and Society, 54*, Article 102001.

Feng, Z., Yu, C., & Cao, S. J. (2019). Fast prediction for indoor environment: Models assessment. *Indoor and Built Environment, 28*, 3–6.

Giorgi, E., Cattaneo, T., Ni, M., & Alatriste, R. (2020). Sustainability and effectiveness of Chinese outline for national tourism and leisure. *Sustainability, 12*, 1161.

Gronemeier, T., & Sühring, M. (2019). On the effects of lateral openings on courtyard ventilation and pollution-A large-eddy simulation study. *Atmosphere, 10*, 63.

Gupta, J., Lin, C. H., & Chen, Q. (2010). Characterizing exhaled airflow from breathing and talking. *Indoor Air, 20*, 31–39.

Hao, S., Yu, C., Xu, Y., & Song, Y. (2019). The effects of courtyards on the thermal performance of a vernacular house in a hot-summer and cold-winter climate. *Energies, 12*, 1042.

Hong, B., & Lin, B. (2015). Numerical studies of the outdoor wind environment and thermal comfort at pedestrian level in housing blocks with different building layout patterns and trees arrangement. *Renewable Energy, 73*, 18–27.

Hvelplund, M., Liu, L., Frandsen, K., Qian, H., Nielsen, P., Dai, L., et al. (2019). Numerical investigation of the lower airway exposure to indoor particulate contaminants. *Indoor and Built Environment, 29*, 575–586.

Khalili, M., & Amindeldar, S. (2014). Traditional solutions in low energy buildings of hot-arid regions of Iran. *Sustainable Cities and Society, 13*, 171–181.

Kubota, T., Zakaria, M., Abe, S., & Toe, D. (2017). Thermal functions of internal courtyards in traditional Chinese shophouses in the hot-humid climate of Malaysia. *Building and Environment, 112*, 115–131.

Li, J., Liu, J., Srebric, J., Hu, Y., Liu, M., Su, L., et al. (2019). The effect of tree-planting patterns on the microclimate within a courtyard. *Sustainability, 11*, 1–21.

Liu, S., Pan, W., Zhao, X., Zhang, H., Cheng, X., Long, Z., et al. (2018). Influence of surrounding buildings on wind flow around a building predicted by CFD simulations. *Building and Environment, 140*, 1–10.

Micallef, D., Buhagiar, V., & Borg, S. (2016). Cross-ventilation of a room in a courtyard building. *Energy and Buildings, 133*, 658–669.

Mousa, W., Lang, W., & Auer, T. (2017). Numerical assessment of the efficiency of fenestration system and natural ventilation mechanisms in a courtyard house in hot climate. *Building Simulation, 10*, 737–754.

Nasrollahi, N., Hatami, M., Khastar, S., & Taleghani, M. (2017). Numerical evaluation of thermal comfort in traditional courtyards to develop new microclimate design in a hot and dry climate. *Sustainable Cities and Society, 35*, 449–467.

Ng, L., Zimmerman, S., Good, J., Toll, B., Emmerich, S., & Persily, A. (2019). Estimating real-time infiltration for use in residential ventilation control. *Indoor and Built Environment, 29*, 508–526.

Qi, D., Cheng, J., Katal, A., Wang, L., & Athienitis, A. (2019). Multizone modelling of a hybrid ventilated high-rise building based on full-scale measurements for predictive control. *Indoor and Built Environment, 29*, 496–507.

Ren, C., & Cao, S. J. (2019). Development and application of linear ventilation and temperature models for indoor environment prediction and HAVC systems control. *Sustainable Cities and Society, 51*, Article 101673.

Ren, C., & Cao, S. J. (2020). Implementation and visualization of artificial intelligent ventilation control system using fast prediction models and limited monitoring data. *Sustainable Cities and Society, 52*, Article 101860.

Ren, J., & Cao, S. J. (2020). Development of self-adaptive low-dimension ventilation models using OpenFOAM: Towards the application of CFD incorporated into AI. *Building and Environment, 171*, Article 106671.

Richards, P., & Hoxey, R. (1993). Appropriate boundary conditions for computational wind engineering models using the k-ε turbulence model. *Journal of Wind Engineering and Industrial Aerodynamics, 46&47*, 145–153.

Santiago, J., Martilli, A., & Martín, F. (2007). CFD simulation of airflow over a regular array of cubes. Part I: Three-dimensional simulation of the flow and validation with wind-tunnel measurements. *Boundary-Layer Meteorol, 122*, 609–634.

Shih, T., Liou, W., Shabbir, A., Yang, Z., & Zhu, J. (1995). A new k-ε eddy-viscosity model for high Reynolds number turbulent flows-model development and validation. *Computer & Fluids, 24*, 227–238.

Soflaei, F., Shokouhian, M., Abraveshdar, H., & Alipour, A. (2017). The impact of courtyard design variants on shading performance in hot- arid climates of Iran. *Energy and Buildings, 143*, 71–83.

Subhashini, S., & Thirumaran, K. (2019). CFD simulations for examining natural ventilation in the learning spaces of an educational building with courtyards in Madurai. *Building Services Engineering Research and Technology* Accepted.

Taleb, H., Wriekat, T., & Hashaykeh, H. (2020). Optimising natural ventilation using courtyard strategies: CFD simulation of a G+1 office building in Madinah. *International Journal of Sustainable Energy* Accepted.

Teshnehdel, S., Mirnezami, S., Saber, A., Pourzangbar, A., & Olabi, A. G. (2020). Data-driven and numerical approaches to predict thermal comfort in traditional courtyards. *Sustainable Energy Technologies and Assessments, 37*, Article 100569.

Wang, Q. (2014). *Research on the wind environment of traditional dewellings and optimization in Tongli*Thesis. Nanjing, China: Southeast University.

Wang, H., Karava, P., & Chen, Q. (2015). Development of simple semi-empirical models for calculating airflow through hopper, awning, and casement windows for single-sided natural ventilation. *Energy and Buildings, 96*, 373–384.

Xu, C., & Liu, L. (2018). Personalized ventilation: One possible solution for airborne infection control in highly occupied space? *Indoor and Built Environment, 27*, 873–876.

Xu, C., Luo, X., Yu, C., & Cao, S.-J. (2020). The 2019-nCoV epidemic control strategies and future challenges of building healthy smart cities. *Indoor and Built Environment, 29*, 639–644.

Xu, X., Luo, F., Wang, W., Hong, T., & Fu, X. (2018). Performance-based evaluation of courtyard design in China's cold-winter hot-summer climate regions. *Sustainability, 10*, 1–19.

Yang, L., Liu, X., Qian, F., & Niu, S. (2020). Research on the wind environment and air quality of parallel courtyards in a university campus. *Sustainable Cities and Society, 56*, Article 102019.

Zahra, Z., Shahin, H., & Pirouz, H. (2018). Reviewing the thermal and microclimatic function of courtyards. *Renewable and Sustainable Energy Reviews, 93*, 580–595.

Zhai, Z., Xue, Y., & Chen, Q. (2014). Inverse design methods for indoor ventilation systems using CFD-based multi-objective genetic algorithm. *Building Simulation, 7*, 661–669.

Zhao, B., Chen, C., & Tan, Z. (2009). Modeling of ultrafine particle dispersion in indoor environments with an improved drift flux model. *Journal of Aerosol Science, 40*, 29–43.